Mon. Not. R. Astron. Soc. **415,** 3616–3626 (2011) doi:10.1111/j.1365-2966.2011.18978.x

Analysing derived metallicities and ionization parameters from model-based determinations in ionized gaseous nebulae

O. L. Dors Jr,[1⋆] Angela Krabbe,[1] Guillermo F. Hägele[2,3] and Enrique Pérez-Montero[4]

[1] *Universidade do Vale do Paraíba, Av. Shishima Hifumi, 2911, Cep 12244-000, São José dos Campos, SP, Brazil*
[2] *Facultad de Ciencias Astronómicas y Geofísicas, Universidad Nacional de la La Plata, Paseo del Bosque s/n, 1900 La Plata, Argentina*
[3] *Departamento de Física Teórica, C-XI, Universidad Autónoma de Madrid, 28049 Madrid, Spain*
[4] *Instituto de Astrofśica de Andalucúa (CSIC), PO Box 3004, 18080 Granada, Spain*

Accepted 2011 April 28. Received 2011 April 27; in original form 2011 February 18

ABSTRACT

We analyse the reliability of oxygen abundances and ionization parameters obtained from a number of diagnostic diagrams. To do this, we used the literature to compile the observational emission-line intensities and oxygen abundances of 446 star-forming regions whose O/H abundances were determined by direct estimation of the electron temperature. These compiled abundances were compared with the values calculated in this work using various diagnostic diagrams in combination with results from a grid of photoionization models. We found that the [O III]/[O II] versus [N II]/[O II], [O III]/Hβ versus [N II]/[O II] and ([O III]/Hβ)/([N II]/Hα) versus [S II]/[S III] diagnostic diagrams gave O/H values close to those obtained using the electron temperature, with differences of about 0.04 dex and a dispersion of about 0.3 dex. Similar results were obtained by detailed models, but with a dispersion of 0.08 dex. The origin of the dispersion found with the use of diagnostic diagrams is probably the differences between the real N/O–O/H relation of the sample and the one assumed in the models. This is confirmed by the use of detailed models that do not have a fixed N/O–O/H relation. We found no correlation between the ionization parameter and metallicity for the objects of our sample. We conclude that the combination of two line ratios predicted by photoionization models, one sensitive to the metallicity and the other sensitive to the ionization parameter, which takes into account the physical conditions of star-forming regions, gives O/H estimates close to the values derived using direct detections of electron temperature.

Key words: galaxies: abundances – galaxies: evolution – galaxies: formation – galaxies: general – galaxies: ISM.

1 INTRODUCTION

Oxygen abundance estimates in star-forming regions play a crucial role in our understanding of galaxy evolution. For example, oxygen radial gradients in spiral galaxies obtained by H II region observations (e.g. Stanghellini et al. 2010; Kewley et al. 2010; Bresolin et al. 2009; Krabbe et al. 2008; Dors & Copetti 2005; Kennicutt, Bresolin & Garnett 2003) are essential for testing chemical evolution models (see Mollá & Díaz 2005) and for investigating both the effect of environment on galaxy interactions (Ellison et al. 2010; Dors & Copetti 2006; Skillman et al. 1996) and the mass–metallicity relation of galaxies (e.g. Pilyugin, Vílchez & Contini 2004; Pérez-Montero & Contini 2009). Likewise, oxygen abundance estimates in metal-poor galaxies are important for testing theories concerning the chemical evolution of galaxies, because these are the least chemically evolved objects in the Universe (Kunth & Sargent 1983).

Unfortunately, for most star-forming regions, only collisionally excited emission lines (CELs) in the optical are bright enough to be used for the derivation of elemental abundances. CELs are temperature-sensitive, and thus only an accurate determination of the metallicity can be achieved by estimations of the electron temperature (this method will be called the T_e-method), using, for instance, the ratio of different CELs [O III](λ4959 + λ5007)/λ4363, which are weak or unobservable in star-forming regions with high metallicity and/or low excitation (Dors et al. 2008; Díaz et al. 2007). In these cases, oxygen abundances can be obtained by empirical (i.e. using oxygen determinations via the T_e-method) or theoretical (i.e. using photoionization models) calibrations between oxygen abundances and more easily measured line ratios (hereafter strong-line methods). The oxygen abundance indicator R_{23} = ([O II]λ3727+[O III]λ4959,λ5007)/Hβ proposed by Pagel et al. (1979) has found wide acceptance in this context, and

⋆E-mail: olidors@univap.br

several authors have calibrated this line ratio with O/H abundance (e.g. Edmunds & Pagel 1984; Dopita & Evans 1986; Pilyugin 2001; Dors & Copetti 2005). Additional O/H indicators based on other emission lines such as N_2 = [N II]λ6584/Hα (Storchi-Bergmann, Calzetti & Kinney 1994), [N II]λ6584/[O III]λ5007 (Alloin et al. 1979), S_{23} = ([S II]λλ6716,6731+[S II]λλ9069,9532)/Hβ (Vílchez & Esteban 1996; Díaz & Pérez-Montero 2000) have also been suggested (see also Kewley & Dopita 2002). However, different methods or different calibrations of the same oxygen indicator provide different oxygen values, with discrepancies of up to 1.0 dex (Kewley & Ellison 2008; Rupke, Veilleux & Baker 2008; Dors & Copetti 2005; Kennicutt, Bresolin & Garnett 2003). The large number of direct oxygen estimates available in the literature has enabled this discrepancy to be investigated. For example, Yin et al. (2007) determined the gas-phase oxygen abundance for a sample of 695 galaxies and H II regions using the T_e-method and compared these determinations with the ones via R_{23}, N_2, ([N II]λ6584/Hα)/([O III]λ5007/Hβ) and [S II](λ6717+λ6731)/Hα. They found that, among the indices above, N_2 provides more consistent O/H abundances when compared with the ones from the T_e-method. Similar analyses were also carried out by Pérez-Montero & Díaz (2005), Liang et al. (2006) and Nagao, Maiolino & Marconi (2006).

The studies above analysed strong-line methods based mainly on one line ratio, such as the R_{23} or N_2, among others. In principle, the use of diagnostic diagrams, containing line ratios strongly dependent on the degree of ionization and on the metallicity of star-forming regions, suggested by Baldwin, Phillips & Terlevich (1981) to separate objects according to their primary excitation mechanisms, can improve the accuracy of strong-line methods. Although a large number of these diagrams have been applied to estimate the oxygen abundances and ionization parameters of star-forming regions (e.g. Levesque, Kewley & Larson 2010; Viironen et al. 2007; Kewley et al. 2001; McGaugh 1991; Dors et al. 2008; Dopita & Evans 1986), a comparison of oxygen estimates obtained from these diagrams and the T_e-method is unavailable in the literature.

Another important issue related to the determination of metallicity using strong-line methods is the relation between the ionization parameter and the metallicity, which is still controversial. For example, Garnett et al. (1997), in a study of the interstellar abundance gradient in NGC 2403, found that any correlation between the ionization parameter and abundance must be a weak one. This result is in agreement with that obtained by Kennicutt & Garnett (1996) from measurements of the [S II]/[S III] ratio in 41 H II regions in M101, and with that found for three barred galaxies by Dors & Copetti (2005). On the other hand, Bresolin, Kennicutt & Garnett (1999) found that in metal-poor disc H II regions the ionization parameter is about four times larger than that in H II regions with solar metallicity. This relation was also found by Maier et al. (2006) and Nagao et al. (2006) for a sample of galaxies. This subject is important in studying the association of the mass–metallicity relation with the mass–age relation in local galaxies, and the relation between gas metallicity and stellar metallicity (Nagao et al. 2006). Additional analysis using several methods would help to elucidate this disagreement.

In this paper, we employ a grid of photoionization models and data compiled from the literature to estimate oxygen abundances using diagnostic diagrams, and then compare the results with those obtained using the T_e-method. We also investigate the relation of the ionization parameter to the metallicity. Detailed photoionization models are also built to produce more precise determinations of these parameters. In Section 2, we describe the observational data used in the analysis. The modelling procedures are presented in Section 3. A description of the diagnostic diagrams employed is given in Section 4. The results and discussion are presented in Sections 5 and 6, respectively. A conclusion is given in Section 7.

Table 1. Emission-line ratios considered.

Symbol	Definition
R_{23}	([O II]λ3727+[O III]λ4959,λ5007)/Hβ
[O III]/Hβ	[O III]λ5007/Hβ
[O III]/[O II]	[O III]λ5007/[O II]λ3727
[N II]/Hα	[N II]λ6584/Hα
[N II]/[O II]	[N II]λ6584/[O II]λ3727
[S II]Hα	([S II]λ6716+λ6731)/Hα
[S II]/[S III]	([S II]λ6716+λ6731)/([S III]λ9069+λ9532)

2 OBSERVATIONAL DATA

Observational emission-line intensities of a sample of H II galaxies and H II regions and the oxygen abundances computed using the T_e-method were compiled from literature.

The emission lines considered in our analysis are listed in Table 1. This compilation includes data from H II regions obtained by Kennicutt et al. (2003), Bresolin, Garnett & Kennicutt (2004), Lee & Skillman (2004), Bresolin et al. (2005), Bresolin (2007) and Bresolin et al. (2009). The data on H II galaxies were obtained by Guseva, Izotov & Thuan (2000), Vílchez & Iglesias-Páramo (2003), Lee, Salzer & Melbourne (2004), Izotov & Thuan (2004), Izotov et al. (2006) and Hägele et al. (2008). The sample consists of 446 objects (86 H II regions and 360 H II galaxies) whose O/H abundances are in the range $7.0 < 12 + \log(\mathrm{O/H})_{T_e} < 9.0$ and represents practically the entire metallicity range of star-forming regions (see Pilyugin, Contini & Vílchez 2004a). The objects of the sample have $z < 0.07$ and measurements corrected by dust extinction, and no active galactic nucleus or gas-shock contributions are present in their ionization.

3 PHOTOIONIZATION MODELS

3.1 Model grid

To enable the estimation of the oxygen abundance and the ionization parameter using diagnostic diagrams, we employed the photoionization code CLOUDY 8.00 (Ferland 2002) to build a grid of models covering a large space of nebular parameters. In these models, a stellar cluster was assumed to be responsible for the ionization of the nebulae, with a spectral energy distribution (SED) obtained using *Starburst99* (Leitherer et al. 1999). We built models with stellar clusters formed by instantaneous burst with a Salpeter initial mass function ($\alpha = -2.35$), lower and upper stellar mass limits of 0.1 $M_\odot$ and 100 $M_\odot$, respectively, and an age of 2.5 Myr. Other papers that have considered stellar clusters as ionizing sources in order to reproduce strong forbidden lines of the H II region (Copetti, Pastoriza & Dottori 1985; Bresolin, Kennicutt & Garnett 1999; Dopita et al. 2000; Stasińska & Izotov 2003; Dors & Copetti 2005) have derived similar ages for star-forming regions (i.e. 1–3 Myr). Similar ages have also been found from optical photometric data of giant H II regions (e.g. Mayya & Prabhu 1996). Selection effects may explain this limited range of ages. H II regions younger than about 1 Myr are difficult to detect in the optical because they are generally embedded in dusty molecular clouds, which cause considerable

optical extinction. Nebulae older than about 5 Myr are also difficult to observe because their original massive stars have cooled or are dead (Copetti, Pastoriza & Dottori 1985; Garca-Vargas, Bressan & Díaz 1996; Dopita et al. 2000). We used the stellar evolution models from the Geneva group with high mass-loss rates and without stellar rotation (Meynet et al. 1994). The non-local thermodynamic equilibrium (non-LTE) atmosphere model of Pauldrach, Hoffmann & Lennon (2001) was assumed in the models. If a LTE atmosphere model is assumed instead of a non-LTE model, a lower ionization degree is produced in the hypothetical nebulae (Stasińska & Schaerer 1997; Dors & Copetti 2003). This would affect mainly the ionization parameter rather than metallicity determinations for strong-line methods. The models were built having an ionization parameter ranging from $\log U = -1.5$ to -3.5 (with a bin size of 0.5 dex), metallicities (traced by the oxygen abundance) $Z = 0.04$, 0.02, 0.008, 0.004 and 0.001, plane-parallel geometry and an electron density of $N_e = 200\,\mathrm{cm}^{-3}$. This electron density value is typical of non-evolved H II regions (Copetti et al. 2000).

The abundances of heavy metals in the nebula were scaled linearly to the solar metal composition through the comparison of the oxygen abundances, with the exception of the N abundance, which was taken from the relation $\log(\mathrm{N/O}) = \log(0.034+120\,\mathrm{O/H})$ of Vila-Costas & Edmunds (1993). The solar composition ($Z = 0.02$) refers to Allende Prieto, Lambert & Asplund (2001) and corresponds to $12+\log(\mathrm{O/H}) = 8.69$. The presence of internal dust was considered, and the grain abundances (van Hoof et al. 2001) were linearly scaled with the oxygen abundance. To take the depletion of refractary elements onto dust grains into account, the abundances of the elements Mg, Al, Ca, Fe, Ni and Na were reduced by a factor of 10, and Si by a factor of 2 (Garnett et al. 1995), relative to the adopted abundances in each model.

The solar metallicity for the stars from the Geneva evolutionary tracks, which corresponds to the old solar oxygen abundance value [$12+\log(\mathrm{O/H}) = 8.87$ (Grevesse & Sauval 1998)], is higher than the value adopted for the nebular component. This produces an imperfect match between gas and star metallicity in our photoionization models. As pointed out by Dopita, Fischera & Sutherland (2006), the main effect of this is that the computed stellar UV photon field result is slightly softer. To investigate how this discrepancy affects our results, we built a model with a perfect match between nebular and stellar metallicities and compared the results with those of another model whose metallicities were in disagreement. This latter model was built using a SED with $12+\log(\mathrm{O/H}) = 8.69$, obtained by linear interpolation of the spectra with $Z = 0.02$ and $Z = 0.008$. In Fig. 1, we show a histogram with a comparison of some emission-line ratio intensities predicted by these models. We can see that, with the exception of [O III]/[O II] and [O III]/Hβ, the intensities of the majority of the line ratios show little variation when the stellar metallicity of the atmosphere changes. Similarly, the predicted value of the R_{23} index (not shown in Fig. 1) shows a small deviation (i.e. about 12 per cent), which corresponds to variations in the oxygen abundance from calibrations using this line ratio by only 0.02 dex. Thus, the disagreement between the nebular and stellar metallicity has little influence on the Z determinations from strong-line methods and can only affect U estimates in diagnostic diagrams that use [O III]/[O II] and [O III]/Hβ. Interestingly, Dopita et al. (2006) found that critical line ratios changed by 0.1 dex or less, except for the [O I]λ6300/Hα ratio, when a test model with a 0.4 $Z_\odot$ spectral synthesis cluster model from *Starburst99* embedded in a nebula with 1.0 $Z_\odot$ ($12+\log(\mathrm{O/H}) = 8.66$) is run. In the rest of this paper, the solar abundance adopted refers to $12+\log(\mathrm{O/H}) = 8.69$, from Allende Prieto et al. (2001).

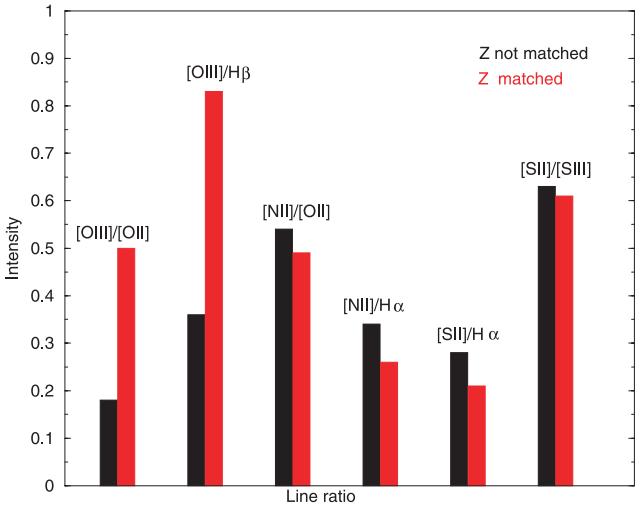

Figure 1. Comparison of some predicted line-ratio intensities from photoionization models with nebular and stellar metallicity matched (red) and not matched (black).

These models are similar to the ones of Dors & Copetti (2006) and have been successful in describing observational data from H II regions (see Dors et al. 2008; Krabbe et al. 2008; Krabbe, Rembold & Pastoriza 2007).

3.2 Detailed models

In general, grids of photoionization models are built assuming a fixed N/O–O/H relation. However, this constancy can yield large uncertainties in O/H estimates from strong-line methods (Pérez-Montero & Contini 2009). This problem can be circumvented by the use of detailed photoionization models. To analyse the source of these uncertainties, we built detailed models in order to reproduce the observational emission-line intensities of 11 H II regions (see Table 2) located along the disc of the galaxy M101, observed by Kennicutt et al. (2003), and we compared our estimates with O/H and U values from other methods. These objects were selected because they cover the wide range in metallicity and ionization parameter considered in this paper. We computed individual models for each object adopting the following methodology. First, a model for each region was built by initially guessing the Z and U values derived from a comparison between the grid of photoionization models shown in the diagnostic diagram [O III]/[O II] versus [N II]/[O II] (see Fig. 2) and the observational data. The electron density of each model was considered to be that computed utilizing the task 'temden' of the package IRAF, where we consider the sulphur ratio [S II]λ6716/[S II]λ6731 and the electron temperature for the O^+ ion measured by Kennicutt et al. (2003). The stellar cluster was assumed to have an age of 2.5 Myr, upper limit mass of 100 $M_\odot$, and metallicity was matched with the closest nebular one assumed in the models. Then, we ran new models with a range for the O/H and U values of 0.3 and 0.5 dex, respectively, with a step of 0.1 dex. From this series of models we selected the model that produced the smallest $\sum \chi_i^2 = \chi^2_{[\mathrm{O\,II}]/\mathrm{H}\beta} + \chi^2_{[\mathrm{O\,III}]/\mathrm{H}\beta}$, where $\chi_i = (I^i_{\mathrm{obs}} - I^i_{\mathrm{pred}})^2/I^i_{\mathrm{obs}}$; I^i_{obs} and I^i_{pred} are the observational and predicted intensities of the line ratios, respectively. Another series of models was computed considering the O/H and U values found by the criterion above but with a range for the N/H and S/H abundances of 0.3 dex in order to reproduce the intensities of the [N II]λ6584 and [S II]λ6720

Table 2. Final parameters of the detailed photoionization models for H II regions observed by Kennicutt et al. (2003).

H II region	12+log(O/H)	log(N/O)	log(S/O)	log U	N_e (cm $^{-3}$)	Age (Myr)
H 1013	8.48	−0.72	−1.34	-1.94	47	2.5
H 1105	8.71	−1.06	−1.64	−2.35	248	1.0
H 1159	8.80	−1.28	−1.94	−2.55	5	1.0
H 1170	8.07	−0.83	−1.31	−2.60	9	2.5
H 1176	8.16	−0.76	−1.38	−2.05	33	2.5
H 1216	8.00	−1.28	−1.64	−2.52	33	1.0
H 336	8.75	−0.80	−1.58	−2.68	15	2.5
H 409	8.53	−1.15	−1.58	−2.37	213	1.0
H 67	8.00	−1.15	−1.64	−2.82	10	2.5
N 5471-D	8.10	−1.15	−1.64	−2.4	110	2.5
S DH323	7.76	−1.45	−1.61	−2.91	61	2.5

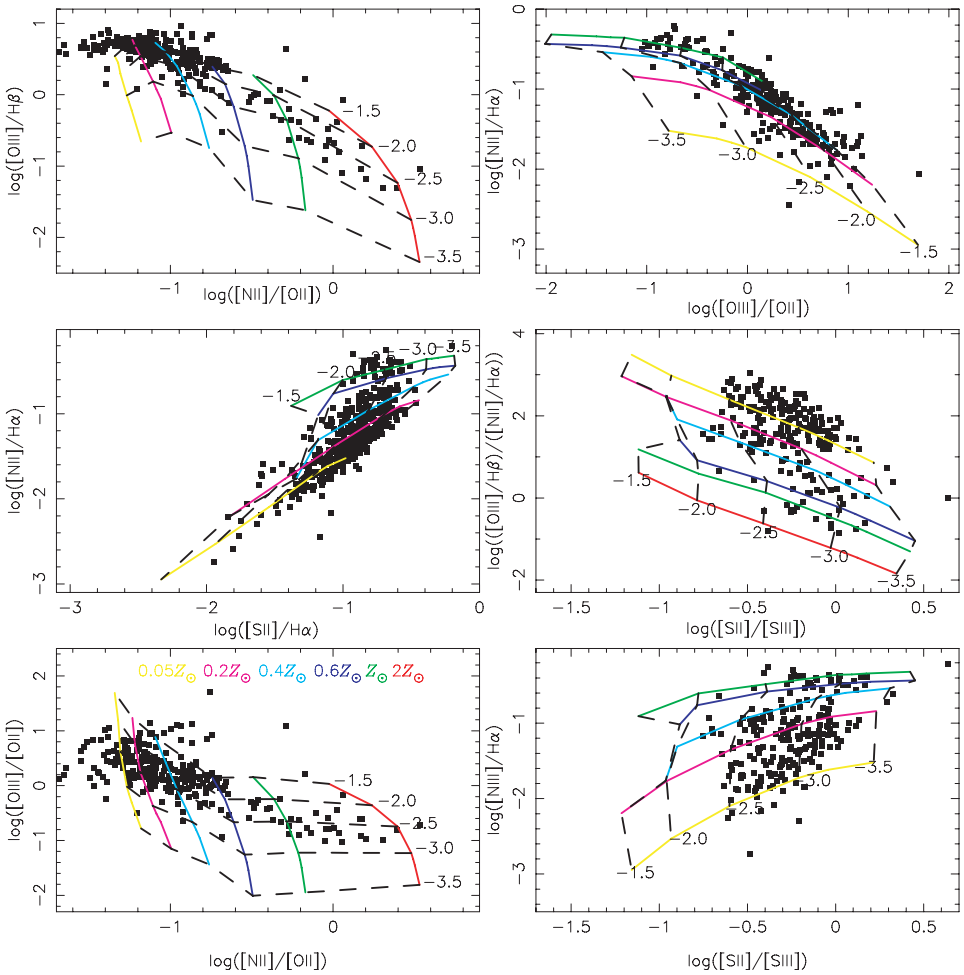

Figure 2. Diagnostic diagrams containing observational data taken from the literature (see Section 2) and results of the grid of photoionization models (see Section 3). The solid lines connect curves of iso-Z, while the dashed lines connect curves of iso-U. The values of log U and Z are indicated. Squares are the observational data. The line ratio used in each plot is defined in Table 1. The typical error bar (not shown) of the emission-line ratio is about 10 per cent.

emission lines. The satisfactory solution is when $I_{\rm pred}$ reproduces $I_{\rm obs}$ within the observational uncertainties and the model has the smallest $\sum \chi_i^2 = \chi^2_{[\rm O\,II]/H\beta} + \chi^2_{[\rm O\,III]/H\beta} + \chi^2_{[\rm N\,II]/H\beta} + \chi^2_{[\rm S\,II]/H\beta}$. In some cases no satisfactory solution was reached considering an age of the ionizing cluster of 2.5 Myr. For these cases, it was necessary to assume an age of 1 Myr because the observed emission lines could only be reproduced by means of a harder SED. In Table 2, we present the final parameters obtained for the models.

4 DIAGNOSTIC DIAGRAMS

We employ six diagnostic diagrams containing predicted and observed emission-line ratios sensitive to Z and U. The diagrams considered are described below.

[O III]/[O II] versus [N II]/[O II] – This diagnostic diagram was suggested by Dopita et al. (2000), where the [O III]/[O II] has a strong dependence on U, on the effective temperature of the ionizing

stars (e.g. Dors & Copetti 2003; Pérez-Montero & Díaz 2005) and on the metallicity (Dopita et al. 2000; Kewley & Dopita 2002). The [N II]/[O II] correlates strongly with Z above to $Z > 0.04\,Z_{\odot}$ (Kewley & Dopita 2002); it is also dependent on the N/O abundance ratio (Pérez-Montero & Contini 2009) and is almost independent of U (Kewley & Dopita 2002).

[N II]/Hα versus [S II]/Hα – This diagram was proposed by Viironen et al. (2007) to estimate the metallicity, where both line ratios are dependent on U and Z (Storchi-Bergmann et al. 1994; Kewley & Dopita 2002). Mazzuca et al. (2006) pointed out that the use of diagnostic diagrams using [N II]/Hα can yield degenerate values for Z, as star-forming regions with low Z and U have [N II]/Hα values similar to regions with high Z and U. In addition, no consistent values were found for over-solar abundances because the [N II]/Hα parameter saturates in this high-metallicity regime. Therefore, we did not consider models with over-solar metallicities. For [S II]/Hα, this line ratio is strongly dependent on U and increases with abundance for low metallicities (Levesque et al. 2010).

[O III]/Hβ versus [N II]/[O II] – This diagram was proposed by Dopita et al. (2000). [O III]/Hβ was suggested by Edmunds & Pagel (1984) as an O/H indicator. However, owing to its dependence on U (Dopita & Evans 1986; McGaugh 1991) a combination with another line ratio is preferable; otherwise, crude O/H estimates with uncertainties of about 0.5 dex are produced (Kobulnicky, Kennicutt & Pizagno 1999).

[N II]/Hα versus [S II]/[S III] – The [S II]/[S III] ratio was proposed as a U indicator by Díaz et al. (1991) for moderate- to high-metallicity regimes (see also Dopita & Evans 1986), and it has little dependence on Z. The problem in using this line ratio is that it is underestimated by photoionization models (Garnett 1989), especially for high metallicities (Dors & Copetti 2005), so any estimation in this regime is uncertain.

([O III]/Hβ)/([N II]/Hα) versus [S II]/[S III] – Pettini & Pagel (2004) showed that ([O III]/Hβ)/([N II]/Hα) is dependent on Z. Because this line ratio is also dependent on U, we combined it with [S II]/[S III] in order to minimize the uncertainties in Z determinations.

[N II]/Hα versus [O III]/[O II] – We investigate the combination between these line ratios to eliminate the problem existing with the use of [S II]/[S III].

5 RESULTS

In Fig. 2, the diagnostic diagrams described above containing the results of our grid of photoionization models and the data sample are shown. The majority of the observational data falls within the regions occupied by the models. However, in the diagram [O III]/Hβ versus [N II]/[O II] the models predict [O III]/Hβ values lower than the observed ones for the low-metallicity regime and high U values, a result also found for the ([O III]/Hβ)/([N II]/Hα) line ratio. Similar difficulties in modelling metal-poor star-forming regions have been found by other authors. For example, Dopita et al. (2006), who used the same SEDs as in this paper, found that their models did not reproduce the observed emission-line diagnostic ratios of objects with $Z < 0.4\,Z_{\odot}$. Martín-Manjón et al. (2008), using a combination of photoionization models and sets of stellar yields from Gavilán, Buell & Mollá (2005), also found that their models did not reproduce the observational data of most metal-deficient H II galaxies (see also Fernandes, Leão & Lacerda 2003). Kewley et al. (2001) pointed out that this disagreement is because stellar ionizing spectra are not hard enough in the far ultraviolet region, and inclusion of the effects of continuum metal opacities in stellar atmospheres should be a way of improving the accuracy of the models. However, in our work we adopted the stellar atmosphere models of Pauldrach et al. (2001), which include treatments of continuum metal opacities, and this disagreement still occurs. A solution for this problem seems to be to include the effects of rotation in stellar models (see discussion above). The number of points varies in the diagrams because for some data sets not all emission lines considered were observed. For example, in Izotov et al. (2006) the [O II]λ3727 is not observed in 30 per cent of the objects.

For the detailed models, a comparison of the predicted and observed emission-line intensities is listed in Table 3, and Fig. 3 shows the ratio between these. We can see that the models reproduce very well (with differences lower than $\sim$15 per cent) all the observed intensities within the observational uncertainties, with the exception of the [S III]λ9069 + λ9532 and [O III]λ4363 emission lines, which are reproduced only for H 336 and NGC 5471-D, and for NGC 1170 and NGC 1176, respectively. Other works have also found that photoionization models are incapable of reproducing emission-line intensities sensitive to T_e (e.g. Stasińska & Schaerer 1997; Oey et al. 2000). This problem has been attributed to temperature gradients and/or temperature inhomogeneities in nebulae, which are not taken into account in simple photoionization models (see Stasińska 2002) such as the ones used in this paper. Because the [O III]λ4363 emission line has an exponential dependence on the electron temperature, any offset between the electron temperatures in the photoionization models and observed forbidden-line temperatures will have a strong effect on the reproduction of this emission line.

Table 3. Observed intensity lines and those predicted by our detailed models.

H II region	[O II]λ3727		[O III]λ4363		[O III]λ5007		[N II]λ6584		[S II]λ6720		[S III]λ9069 + λ9532	
	Obs.	Mod.	Obs.	Mod.	Obs.	Mod.	Obs.	Mod.	Obs.	Mod.	Obs.	Mod.
H 1013	188 ± 10	185	–	0.20	103 ± 5	105	64.6 ± 3.4	67	28.8 ± 1.1	26	131.6 ± 7.0	171
H 1105	185 ± 10	188	1.4 ± 0.1	0.74	316 ± 17	317	33.4 ± 1.8	34	24.1 ± 0.9	27	126.6 ± 11	139
H 1159	198 ± 10	194	1.9 ± 0.4	0.63	317 ± 17	316	23.6 ± 1.3	25	29.8 ± 1.1	27	97.0 ± 5.5	66
H 1170	308 ± 16	295	1.6 ± 0.2	1.67	201 ± 11	194	44.0 ± 2.3	41	56.7 ± 2.1	51	170.0 ± 9.3	136
H 1176	160 ± 8	153	2.4 ± 0.3	2.74	369 ± 20	357	21.2 ± 1.1	23	23.0 ± 0.8	19	113.5 ± 6.1	137
H 1216	151 ± 8	149	4.7 ± 0.3	6.67	473 ± 25	478	11.0 ± 0.6	9	18.9 ± 0.7	18	83.0 ± 4.6	63
H 336	178 ± 9	183	–	0.02	23 ± 1	26	95.9 ± 5.1	99	56.8 ± 2.1	58	107.0 ± 5.7	102
H 409	218 ± 12	212	2.3 ± 0.2	1.39	370 ± 20	359	27.3 ± 1.4	24	31.2 ± 1.1	28	90.1 ± 4.9	141
H 67	244 ± 13	248	3.5 ± 0.5	4.67	342 ± 18	356	16.3 ± 0.9	19	26.3 ± 1.3	29	92.1 ± 5.7	62
N 5471-D	137 ± 7	140	8.0 ± 0.4	7.10	578 ± 31	574	8.5 ± 0.5	11	20.6 ± 0.8	18	75.7 ± 4.3	75
S DH323	194 ± 10	198	5.5 ± 0.9	3.7	227 ± 12	234	7.9 ± 0.7	7	20.8 ± 1.4	23	–	42

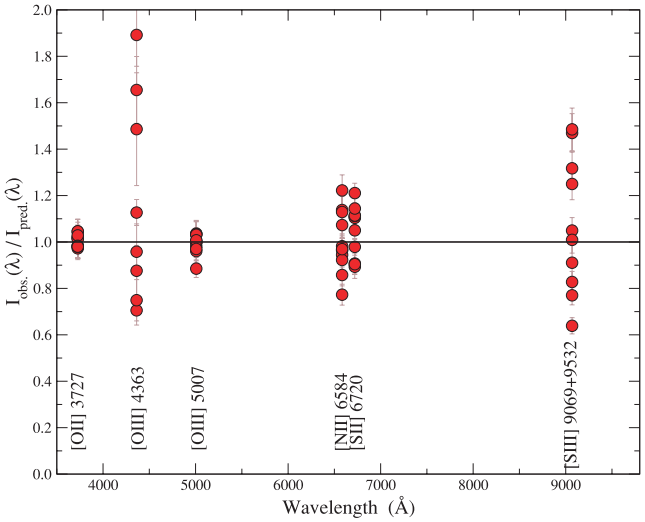

Figure 3. Ratio between observed and predicted emission-line intensities of some H II regions located in M101, as observed by Kennicutt et al. (2003).

5.1 Abundance determination comparison

To check the reliability of diagnostic diagrams, in Figs 4 and 5 we present a comparison of O/H obtained from these methods with O/H abundances obtained from the T_e-method, and the difference between these estimates. We include in Fig. 5 the results of the detailed models for the H II regions in M101, as well as the results of Pérez-Montero et al. (2010), who built detailed photoionization models in order to reproduce the emission-line intensities of 10 H II galaxies. In each plot, the average value ($\overline{D}$) and the dispersion (σ) of this difference are also presented. The O/H and U values from the diagnostic diagrams were obtained by linear interpolation from the model grid shown in Fig. 2. In a few cases, double values of Z and/or U for the same objects are found because the models overlap for a given combination of these parameters. In these cases, the estimations were not considered in our analysis. This occurred mainly for the [N II]/Hα versus [S II]/Hα diagnostic diagram (for about 5 per cent of the points).

The diagnostic diagrams that provide the best results are the [O III]/[O II] versus [N II]/[O II], [O III]/Hβ versus [N II]/[O II] and ([O III]/Hβ)/([N II]/Hα) versus [S II]/[S III], which give O/H estimates close to the T_e-method with an absolute difference of about 0.04 dex. The lowest dispersion is found with the use of the [O III]/Hβ versus [N II]/[O II] diagram. For the majority of the diagrams, the difference and the dispersion are larger in the regime of low metallicity (12+log(O/H) < 8.0). For the other diagrams this difference is about 0.25 dex. The O/H abundances from detailed models are in agreement with the ones obtained with the T_e-method for the objects analysed, and the dispersion derived is lower than the one obtained using diagnostic diagrams.

5.2 Ionization parameter determination

Regarding the ionization parameter, in Fig. 6 we plot U against the oxygen abundances obtained from the diagnostic diagrams presented in Section 4 as well as those obtained from detailed models. The results for H II galaxies and H II regions are indicated by different symbols (red and black squares, respectively). The [O III]/Hβ versus [N II]/[O II] and [O III]/[O II] versus [N II]/[O II] diagrams estimate larger U values than do other methods. There is no clear trend

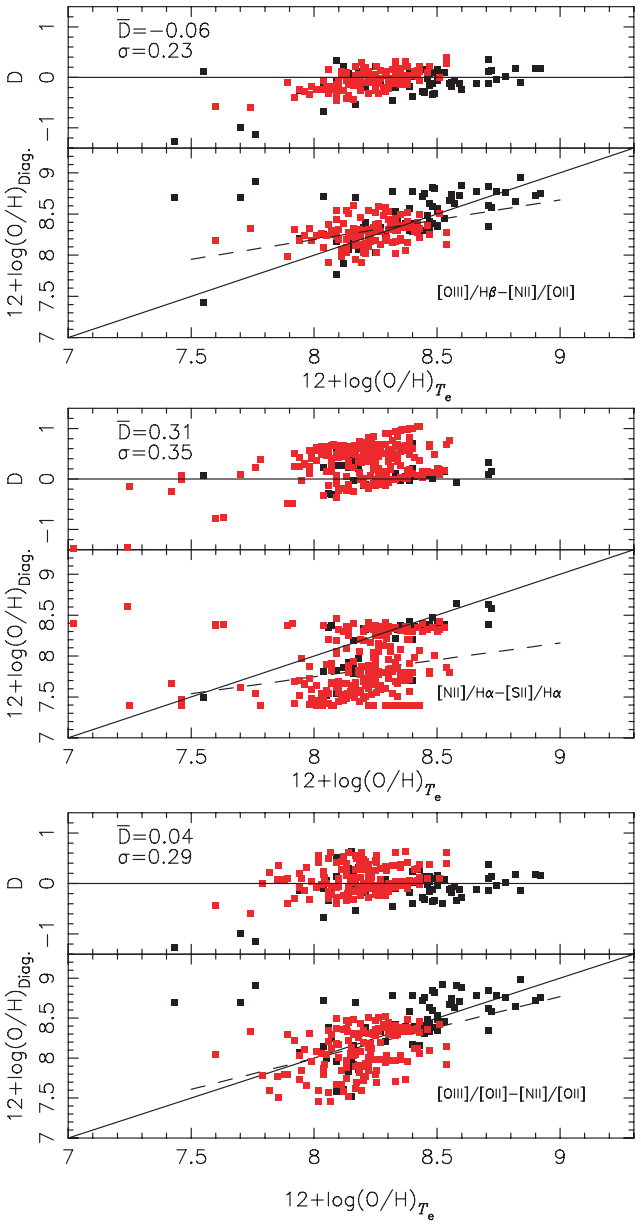

Figure 4. Comparison between the oxygen abundances derived using the T_e-method and those computed using the diagnostic diagrams. In each plot the diagnostic diagrams used to compute the oxygen abundances are indicated. The top panel of each diagram shows the difference between the oxygen abundance from the T_e-method and that from the diagnostic diagrams. The average value of this difference and the dispersion are shown in each plot. Solid lines represent equality of the two estimates. The results for H II galaxies and H II regions are marked by red and black squares, respectively

of U with O/H, and this result is also confirmed by the detailed model estimation.

6 DISCUSSION

Comparing oxygen abundance determinations from the T_e-method for the sample of H II regions and H II galaxies with those based on strong emission lines, we found that the [O III]/[O II] versus [N II]/[O II], [O III]/Hβ versus [N II]/[O II] and ([O III]/Hβ)/([N II]/Hα) versus [S II]/[S III] diagnostic diagrams gave O/H values nearest to

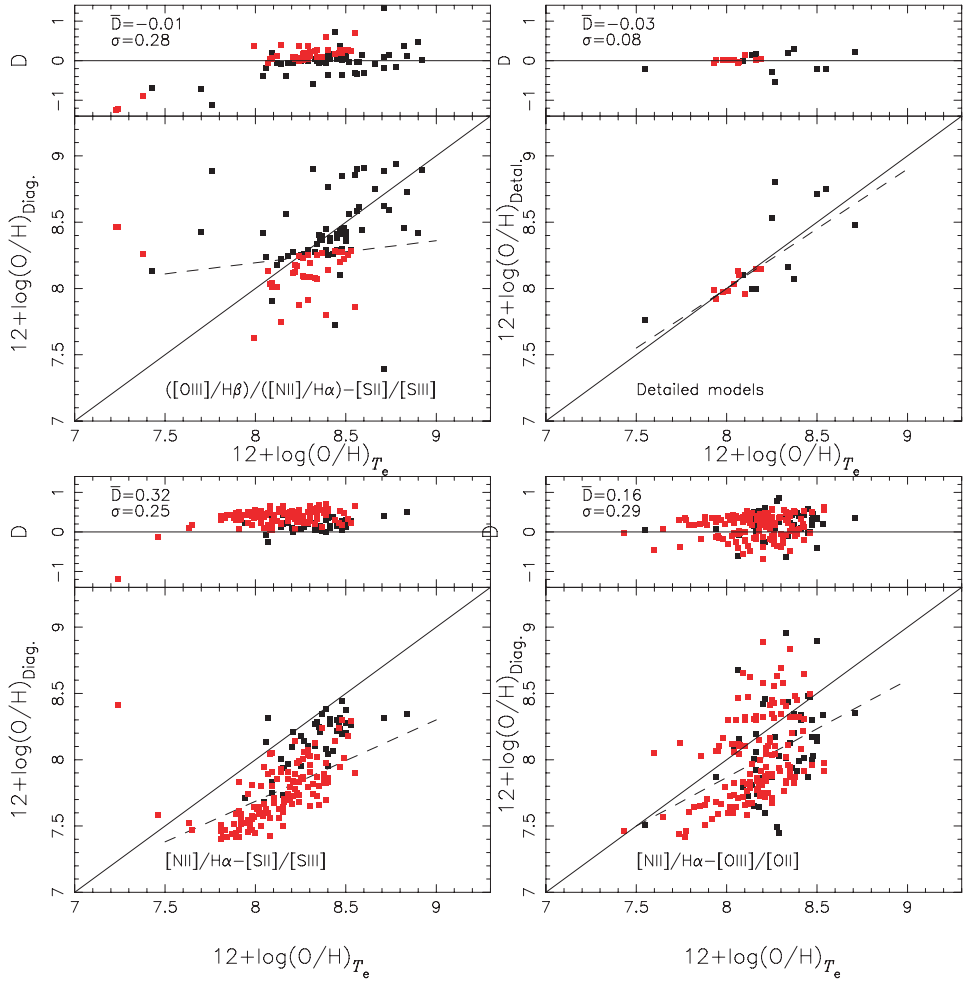

Figure 5. As Fig. 4, but for other diagnostic diagrams. The panel in the top right represents the comparison using detailed photoionization models, and the red points were taken from Pérez-Montero et al. (2010). The results for H II galaxies and H II regions are indicated by different symbols (red and black squares, respectively).

those of the T_e-method, with differences of about 0.04 dex and a dispersion of about 0.30 dex. This difference is about the same as the one between oxygen estimates from the *P*-method (Pilyugin 2001) and from the T_e-method found by López-Sanchez & Esteban (2010) considering a sample of Wolf–Rayet galaxies. It is lower by about 0.15 dex than the estimate found by these authors when using only one emission-line ratio sensitive to metallicity.

As seen in Figs 4 and 5, large difference are found for 12 + log (O/H) < 8.0 ($Z \lesssim 0.2\,Z_\odot$). Similar results were also found by Yin et al. (2007), who compared oxygen estimates from N_2 and ([O III]/Hβ)/([N II]/Hα) with those from the T_e-method for a sample of 695 galaxies and H II regions. This occurs because in this regime of metallicity the nitrogen and oxygen both have mainly a primary nucleosynthesis origin, causing nitrogen emission lines to be relatively independent of oxygen abundance, and consequently the use of metallicity indicators based on these emission lines is not reliable (e.g. Levesque et al. 2010; Dopita et al. 2000).

The origin of the dispersion found by us probably lies in the difference between the real N/O–O/H abundance relation of the object sample and the one assumed in our models. In fact, Pérez-Montero & Contini (2009) analysed the dependence of N/O with O/H estimation obtained through the metallicity indicators using nitrogen line ratios and compared these estimations with the ones obtained with the T_e-method. They found approximately the same dispersion as derived by us, and also showed that if the N/O ratio is taken into account in strong-line methods, the dispersion can be reduced by about 0.1 dex. Moreover, the scattering of N/O for a fixed O/H value is larger for the low-metallicity regime (see e.g. Pilyugin, Thuan & Vílchez 2003), which introduces a larger dispersion for oxygen estimations in this regime, such as the one observed in our results. This is confirmed by the use of detailed models, for which the N/O–O/H relation is a free parameter, yielding a lower dispersion (0.08 dex) than the ones obtained from diagnostic diagrams. Yin et al. (2007) also obtained similar results by comparing oxygen abundances derived from the T_e-method and those obtained with the photoionization models of Charlot & Longhetti (2001).

Another important test is to verify if abundance gradient estimates obtained using diagnostic diagrams agree with those obtained with the T_e-method. Thus, in Fig. 7 we show a comparison of the oxygen gradient slope computed using the [O III]/[O II] versus [N II]/[O II] diagram presented in Fig. 2 and that from the T_e-method for spiral galaxies M101, M51, M33 and NGC 2403 obtained by Kennicutt et al. (2003), Bresolin et al. (2004), Magrini et al. (2007) and Garnett et al. (1997), respectively. We can see that, within the uncertainties given by the linear fitting, the diagnostic diagram yields abundance gradients consistent with the ones obtained with the T_e-method.

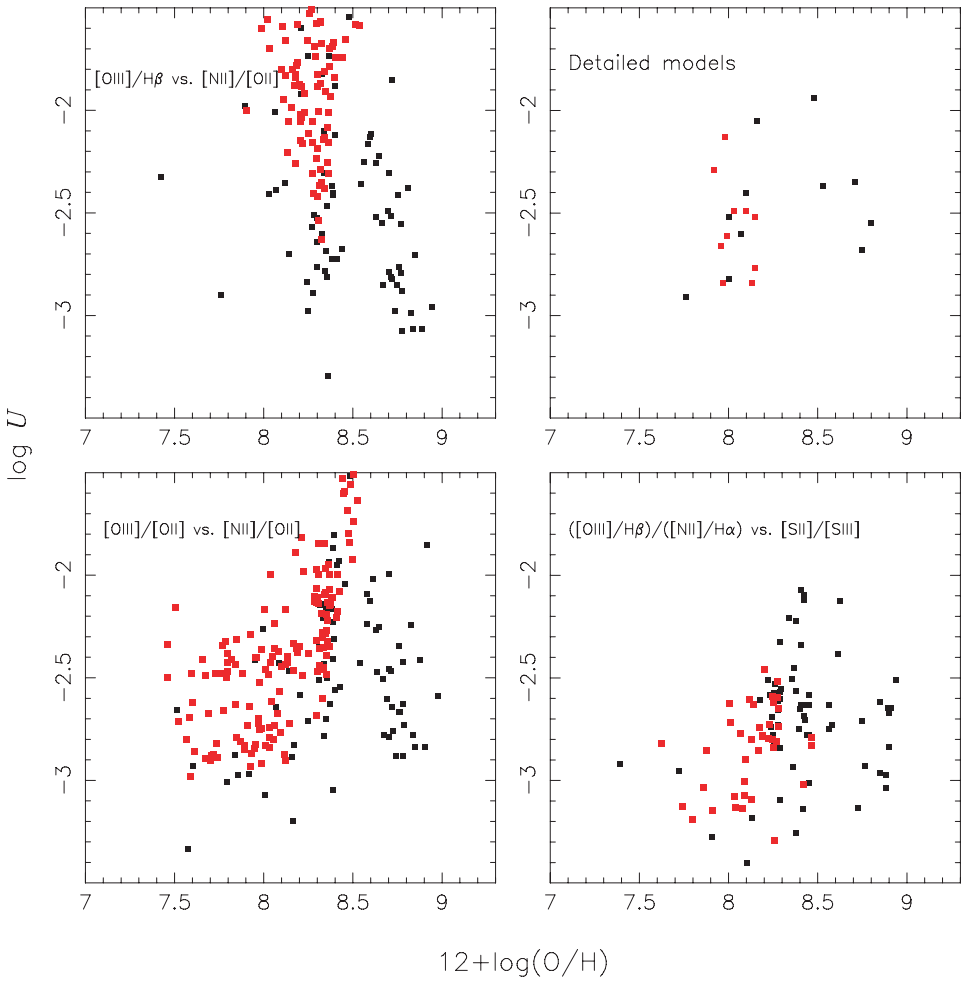

Figure 6. Logarithm of the ionization parameter versus oxygen abundances. Squares represent the results obtained using the diagnostic diagrams indicated in each plot. The results for H II galaxies and H II regions are indicated by different colours (red for H II galaxies and black for H II regions). In the upper right plot the squares represent estimations from detailed photoionization models, with the red points taken from Pérez-Montero et al. (2010).

Again, the difference between the gradient estimates is probably because of the N/O–O/H relation assumed in our models and the one of the galaxies. This is supported by the detailed model results, as a linear fitting on oxygen abundance from these, presented in Table 2, yields a gradient for M101 of $12+\log(\mathrm{O/H}) = 0.90(\pm0.26)\ R/R_{25} + 8.77(\pm0.15)$, the same gradient as found by Kennicutt et al. (2003) using the T_e-method.

In general, oxygen determinations obtained from strong-line methods, which use emission-line intensities predicted by photoionization models, are overestimated by up to 0.5 dex when compared with those obtained from the T_e-method (Stasińska 2002; Kennicutt et al. 2003; Garnett et al. 2004; Dors & Copetti 2005; Kewley & Ellison 2008). This discrepancy is attributed to the fact that photoionization codes are not realistic enough, do not treat all the relevant physical processes correctly, use inaccurate atomic data, etc. (Kennicutt et al. 2003). However, as seen previously, use of state-of-the-art photoionization models and the combination of two line ratios, one sensitive to the metallicity and the other to the ionization parameter, which does take into account the physical conditions (hardness of the ionizing radiation and geometrical factors) of star-forming regions (Pilyugin 2001), minimizes the effects mentioned above and gives O/H estimates close to those from the T_e-method. As explained in Section 3, the match between solar abundances for the gas and star has little influence on metallicity indicators (i.e. [N II]/[O II]), showing that the metallicity estimates from our models are independent of whether or not these values are matched.

The ionization parameter is expected to be dependent on the metallicity because stellar atmospheres of massive O stars become cooler with increasing metallicity as a result of enhanced line and wind blanketing (Massey et al. 2005), leading to a decrease in the ionization parameter. Moreover, when the stellar atmosphere abundance is higher, photons emitted from the photosphere are scattered more efficiently, causing a greater conversion efficiency from luminous energy flux to mechanical energy flux in the stellar wind base region, which leads to a decrease of U in the H II region (Dopita et al. 2006). A decrease of U with increasing Z was found for H II galaxies by Nagao et al. (2006) and Maier et al. (2006), and for disc H II regions by Bresolin et al. (1999). However, our results indicate no systematic dependence of the ionization parameter on the metallicity for the sample of objects considered, although using our grid of models it is impossible to check what factor (e.g. stellar effective temperature, geometrical factors, aging) is responsible for this behaviour. This result is in agreement with findings by Dors & Copetti (2005), Garnett et al. (1997) and Kennicutt & Garnett (1996), who used [S II]/[S III] in order to estimate the ionization parameter in H II regions located in spiral discs. To analyse whether our result

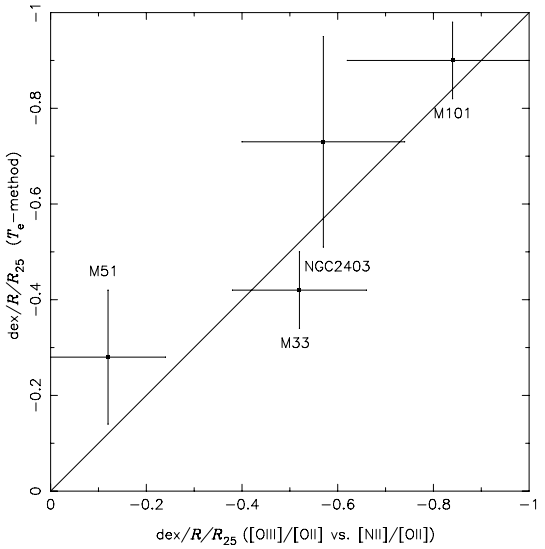

Figure 7. Comparison of abundance gradient slopes derived using the [O III]/[O II] versus [N II]/[O II] and T_e-method for various galaxies, as indicated. The slopes are measured in dex/R/R_{25}, where R_{25} is the isophotal radius. The references from which we collected the gradients for the T_e-method are cited in the text. Solid lines represent equality of the two estimates.

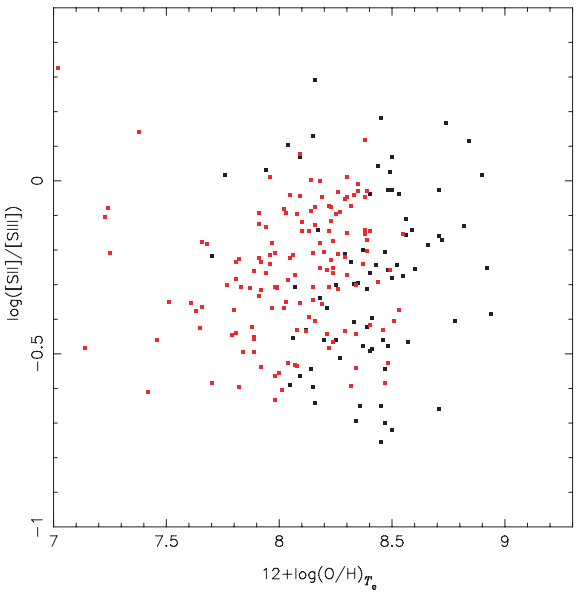

Figure 8. [S II]/[S III] observed line ratio versus oxygen abundance for the T_e-method for our sample of objects. H II galaxies and H II regions are marked with red and black squares, respectively.

is an artefact of the methods used in this paper, in Fig. 8 we plot the [S II]/[S III] line ratio intensity and the O/H abundances obtained by the T_e-method for our sample. Again, there is no systematic behaviour of U with O/H.

As noted from Fig. 6, the [O III]/Hβ versus [N II]/[O II] and [O III]/[O II] versus [N II]/[O II] diagrams indicate very high U values ($\log U > -2$) for some objects, which are not predicted by the detailed model and by the ([O III]/Hβ)/([N II]/Hα) versus [S II]/[S III] diagram. This occurs because photoionization models under-predict the [O III]/Hβ (see Fig. 2), mainly for objects with low metallicity. Because these line ratios are age-dependent, it is possible that models assuming a harder SED would resolve this problem. Thus, we ran a grid of photoionization models (not shown) using as ionizing source a cluster of 1 Myr and computed U and Z values. We found that, for the diagram with [O III]/[O II], this new grid yielded values of U in agreement with the ones from other diagrams. However, for the diagram with [O III]/Hβ, although a better match between the models and the observational data was obtained, the U estimations continued to be overestimated in relation to the ones from other methods. The O/H estimates practically did not change in these cases. A similar problem was pointed out by Stasińska & Izotov (2003), who used a sequence of photoionization models to reproduce the observational data of H II galaxies and found that the models under-predicted [O III]/Hβ for objects with $7.4 < \log(\mathrm{O/H}) < 8.0$. These authors invoked several mechanisms to explain this discrepancy, such as secondary ionization by X-rays and shocks, but a definitive conclusion was not reached. Recently, Levesque et al. (2010) compared the observational data of a large sample of star-forming galaxies with a grid of photoionization models, such as the ones presented in this paper, but considering as the ionizing source stellar clusters with different ages and formed by instantaneous and continuous star formation. Similar to our results, they found that models with very young clusters of 0–1 Myr and formed instantaneously reproduced the observed [O III]/Hβ better than older ones, although better agreement is given by models adopting a continuous star formation history (see also Pérez-Montero et al. 2010). These authors did not compare U estimates obtained by different emission-line ratios, but it is probable that the discrepancy found by us is maintained even using their models with continuous star formation. Levesque et al. (2010) showed that the new generation of Geneva evolutionary tracks, which include stellar rotation, produces a SED more prominent in the higher-energy regime ($\lambda \lesssim 230$ Å) than the one used here, with rotation effects being more important at lower metallicities. Thus, it is probable that if these SEDs were used in our photoionization models, the predicted intensities of the [O III]/Hβ would be larger and U estimates from diagnostic diagrams using this line ratio would coincide with the ones from other diagrams.

As the [S II]/[S III] ratio is weakly dependent on Z, it is useful to calibrate it with U. In Fig. 9, we show the U–[S II]/[S III] relation predicted by our models for the entire range of Z and the relation proposed by Díaz et al. (1991), as well as our results for [S II]/Hα and [O III]/[O II] versus U.

A linear fitting of the average of these photoionization model results produces

$$\log U = -1.36\,(\pm0.07)\log[\mathrm{S\,II}]/[\mathrm{S\,III}] - 3.09\,(\pm0.05), \quad (1)$$

$$\log U = -1.66\,(\pm0.06)\log[\mathrm{S\,II}]/\mathrm{H}\alpha - 4.13\,(\pm0.07), \quad (2)$$

$$\log U = 1.22\,(\pm0.07)\log[\mathrm{O\,II}]/[\mathrm{O\,III}] - 2.25\,(\pm0.05). \quad (3)$$

As can be seen in Fig. 9, the [S II]/Hα ratio is a good U indicator because it shows little variation with metallicity for $Z > 0.2\,Z_\odot$ and uses emission line with wavelength close to each other, being almost independent of the reddening. Our result for the U–[S II]/[S III] relation is in very good agreement with the relation proposed by Díaz et al. (1991).

7 CONCLUSION

We compared oxygen estimates of objects obtained by direct detection of the electron temperature with those obtained from diagnostic

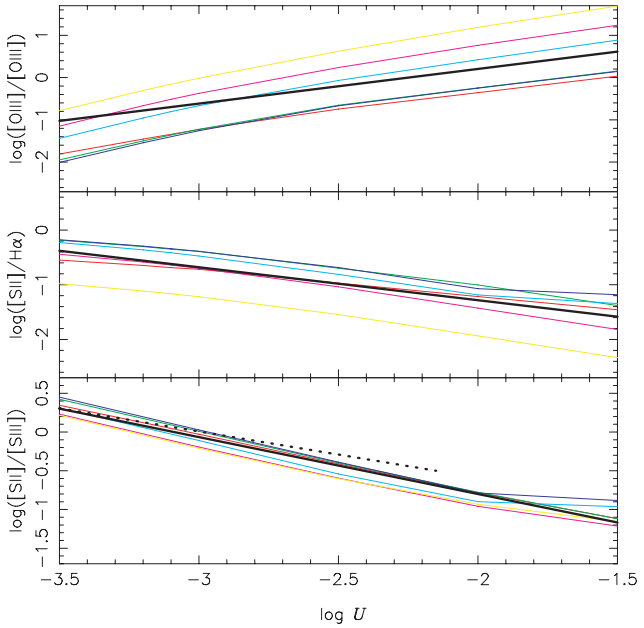

Figure 9. Relation between the ionization parameter U and the [S II]/[S III], [S II]/Hα and [O III]/[S II] line ratios. The coloured solid lines represent results for different metallicities, as in Fig. 2, and the black solid line represents the linear fitting of the average of these results. The dotted line represents the relation proposed by Díaz et al. (1991).

diagrams containing strong emission lines predicted by photoionization models, as well as from detailed models. Among the diagnostic diagrams considered, we found that the ones utilizing the emission lines [O III]/[O II] versus [N II]/[O II], [O III]/Hβ versus [N II]/[O II] and [O III]/Hβ/[N II]/Hα versus [S II]/[S III] gave O/H values nearest to those obtained from the T_e-method, with differences of about 0.04 dex and a dispersion of 0.3 dex. Similar results were obtained using detailed models, but with a smaller dispersion, of 0.08 dex. The origin of the dispersion probably lies in the differences between the real N/O–O relation of the sample and the one assumed in the models. We did not find any correlation of the ionization parameter with the metallicity for the objects in our sample. We conclude that the combination of two line ratios predicted by photoionization models, one sensitive to the metallicity and the other sensitive to the ionization parameter, which takes into account the physical conditions of star-forming regions, gives O/H estimates close to the values derived using direct detections of electron temperatures.

ACKNOWLEDGMENTS

This work was supported by FAPESP under grant 2009/14787-7. GH is grateful to the Spanish Ministerio de Educación y Ciencia for support under grants AYA2007-67965-C03-03 and AYA2010-21887-C04-03, and to the Comunidad de Madrid for support under grant S2009/ESP-1496 (ASTROMADRID). EPM is grateful to the Spanish Ministerio de Ciencia e Innovación for support under grants AYA2007-67965-C03-02 and AYA2010-21887-C04-02, and to the Junta de Andalucía for support under grant TIC114.

REFERENCES

Allende Prieto C., Lambert D. L., Asplund M., 2001, ApJ, 556, L63
Alloin D., Collin-Souffrin S., Joly M., Vigroux L., 1979, A&A, 78, 200
Baldwin J. A., Phillips M. M., Terlevich R., 1981, PASP, 93, 5
Bresolin F., 2007, ApJ, 656, 186
Bresolin F., Kennicutt R. C., Garnett D. R., 1999, ApJ, 510, 104
Bresolin F., Garnett D. R., Kennicutt R. C., 2004, ApJ, 615, 228
Bresolin F., Schaerer D., González Delgado R. M., Stasińska G., 2005, A&A, 441, 981
Bresolin F., Gieren W., Kudritzki R., Pietrzynski G., Urbaneja M. A., Carraro G., 2009, ApJ, 700, 309
Charlot, S., Longhetti M., 2001, MNRAS, 323, 887
Copetti M. V. F., Pastoriza M. G., Dottori H. A., 1985, A&A, 152, 427
Copetti M. V. F., Mallmann J. A. H., Schmidt A. A., Castañeda H. O., 2000, A&A, 357, 621
Díaz A. I., Pérez-Montero E., 2000, MNRAS, 312, 130
Díaz A. I., Terlevich E., Vílchez J. M., Pagel B. E. J., Edmunds M. G., 1991, MNRAS, 253, 245
Díaz A. I., Terlevich E., Castellanos M., Hägele G. F., 2007, MNRAS, 382, 251
Dopita M. A., Evans I. N., 1986, ApJ, 307, 431
Dopita M. A., Kewley L. J., Heisler C. A., Sutherland R. S., 2000, ApJ, 543, 224
Dopita M. A., Fischera J., Sutherland R. S., 2006, ApJS, 167, 177
Dors O. L., Copetti M. V. F., 2003, A&A, 404, 969
Dors O. L., Copetti M. V. F., 2005, A&A, 437, 837
Dors O. L., Copetti M. V. F., 2006, A&A, 452, 437
Dors O. L., Storchi-Bergmann T., Riffel R. A., Schimdt A. A., 2008, A&A, 482, 59
Edmunds M. G., Pagel B. E. J., 1984, MNRAS, 211, 507
Ellison S. L., Patton D. R., Simard L., McConnachie A. W., Baldry I. K., Mendel J. T., 2010, astroph/1002.4418
Ferland G. J., 2002, Hazy, a brief introduction to Cloudy 96.03, Univ. Kentucky, Dept. Phys., Astron. internal report
Fernandes R. C., Leão J. R. S., Lacerda R. R., 2003, MNRAS, 340, 29
Garca-Vargas M. L., Bressan A., Díaz A. I., 1996, A&AS, 112, 13
Garnett D. R., 1989, ApJ, 345, 282
Garnett D. R., Dufour R. J., Peimbert M., Torres Peimbert S., Shields G. A., Skillman E. D., Terlevich E., Terlevich R. J., 1995, ApJ, 449, 77
Garnett D. R., Shields G. A., Skillman E. D., Sagan S. P., Dufour R. J., 1997, ApJ, 489, 63
Garnett D. R., Edmunds M. G., Henry R. B. C., Pagel B. E. J., Skillman E. D., 2004, AJ, 128, 2772
Gavilán M., Buell J. F., Mollá M., 2005, A&A, 432, 861
Grevesse N., Sauval A., 1998, Space Sci. Rev., 85, 161
Guseva N. G., Izotov Y. I., Thuan T. X., 2000, 531, 776
Hägele G. F., Díaz A. I., Terlevich E., Terlevich R., Pérez-Montero E., Cardaci M. V., 2008, MNRAS, 383, 209
van Hoof P. A. M., Weingartner J. C., Martin P. G., Volk K., Ferland G. J., 2001, in Ferland G., Savin D., eds, ASP Conf Ser. Vol. 247, Challenges of Photoionized Plasmas. Astron. Soc. Pac., San Francisco, p. 363
Izotov Y. I., Thuan T. X., 2004, ApJ, 602, 200
Izotov Y. I., Stasińska G., Meynet G., Guseva N. G., Thuan T. X., 2006, A&A, 448, 955
Kennicutt R. C., Jr, Garnett D. R., 1996, ApJ, 456, 504
Kennicutt R. C., Bresolin F., Garnett D. R., 2003, ApJ, 591, 801
Kewley L. J., Dopita M. A., 2002, ApJS, 142, 35
Kewley L. J., Ellison S. L., 2008, ApJ, 681, 1183
Kewley L. J., Dopita M. A., Sutherland R. S., Heisler C. A., Trevena J., 2001, ApJ, 556, 121
Kewley L. J., Rupke D., Zahid H. J., Geller M. J., Barton E. J., 2010, ApJ, 721, L48
Kobulnicky H. A., Kennicutt R. C., Pizagno J. L., 1999, ApJ, 514, 544
Krabbe A. C., Rembold S. B., Pastoriza M. G., 2007, MNRAS, 378, 569
Krabbe A. C., Pastoriza M. G., Winge C., Rodrigues I., Ferreiro D. L., 2008, MNRAS, 389, 1593
Kunth D., Sargent W. L. W., 1983, ApJ, 273, 81
Lee H., Skillman E. D., 2004, ApJ, 614, 698
Lee J. C., Salzer J. J., Melbourne J., 2004, ApJ, 616, 752
Leitherer C., Schaerer D., Goldader J. D. et al., 1999, ApJS, 123, 3
Levesque E. M., Kewley L. J., Larson K. L., 2010, AJ, 139, 712

Liang Y. C., Hammer F., Yin S. Y., Flores H., Rodrigues M., Yang Y. B., 2006, A&A, 473, 411
López-Sanchez A. R., Esteban C., 2010, A&A, 517, 85
McGaugh S. S., 1991, ApJ, 380, 140
Magrini L., Vílchez J. M., Mampaso A., Corradi R. L. M., Leisy P., 2007, A&A, 470, 865
Maier C., Lilly S. J., Carollo C. M., Meisenheimer K., Hippelein H., Stockton A., 2006, ApJ, 639, 858
Martín-Manjón M. L., Mollá M., Díaz A. I., Terlevich R., 2008, MNRAS, 385, 854
Massey P., Puls J., Pauldrach A. W. A., Bresolin F., Kudritzki R. P., Simon T., 2005, ApJ, 627, 477
Mayya Y. D., Prabhu T. P., 1996, AJ, 111, 1252
Mazzuca L. M., Sarzi M., Knapen J. H., Veilleux S., Swaters R., 2006, ApJ, 649, L79
Meynet G., Maeder A., Schaller G., Schaerer D., Charbonnel C., 1994, A&AS, 103, 97
Mollá M., Díaz A. I., 2005, MNRAS, 358, 521
Nagao T., Maiolino R., Marconi A., 2006, A&A, 459, 85
Oey M. S., Dopita M. A., Shields J. C., Smith R. C., 2000, ApJS, 128, 511
Pagel B. E. J., Edmunds M. G., Blackwell D. E., Chun M. S., Smith G., 1979, MNRAS, 189, 95
Pauldrach A. W. A., Hoffmann T. L., Lennon M., 2001, A&A, 375, 161
Pérez-Montero E., Contini T., 2009, MNRAS, 398, 949
Pérez-Montero E., Díaz A. I., 2005, MNRAS, 361, 1063
Pérez-Montero E., García-Benito R., Hägele G. F., Díaz A. I., 2010, MNRAS, 404, 2037
Pettini M., Pagel B. E. J., 2004, MNRAS, 348, L59
Pilyugin L. S., 2001, A&A, 369, 594
Pilyugin L. S., Thuan T. X., Vílchez J. M., 2003, A&A, 397, 487
Pilyugin L. S., Contini T., Vílchez J. M., 2004a, A&A, 423, 427
Pilyugin L. S., Vílchez J. M., Contini T., 2004b, A&A, 425, 849
Rupke D. S. N., Veilleux S., Baker A. J., 2008, ApJ, 674, 172
Skillman E. D., Kennicutt R. C., Shields G. A., Zaritsky D., 1996, ApJ, 462, 147
Stanghellini L., Magrini L., Villaver E., Galli D., 2010, A&A, 521, A3
Stasińska G., 2002, Revista Mexicana de Astronomia y Astrofisia Conf. Ser., 12, 62
Stasińska G., Izotov I., 2003, A&A, 397, 71
Stasińska G., Schaerer D., 1999, A&A, 351, 72
Stasińska G., Schaerer D., 1997, A&A, 322, 615
Storchi-Bergmann T., Calzetti D., Kinney A. L., 1994, ApJ, 429, 572
Viironen K., Delgado-Inglada G., Mampaso A., Magrini L., Corradi R. L. M., 2007, MNRAS, 381, 1719
Vila-Costas M. B., Edmunds M. G., 1993, MNRAS, 265, 199
Vílchez J. M., Esteban C., 1996, MNRAS, 280, 720
Vílchez J. M., Iglesias-Páramo J., 2003, ApJS, 145, 225
Yin S. Y., Liang Y. C., Hammer F., Brinchmann J., Zhang B., Deng L. C., Flores H., 2007, A&A, 462, 535

This paper has been typeset from a TEX/LATEX file prepared by the author.